MEMS Pirani Sensor for Pressure Measurements in the Fine- and High-Vacuum Range

M. Grau[*1,2], F. Völklein[1], A. Meier[1], C. Kunz[1], and P. Woias[2]
[1]RheinMain University of Applied Sciences (Institute for Microtechnologies), [2]University of Freiburg (Department of Microsystems Engineering)
*Corresponding author: Am Brückweg 26,65428 Rüsselsheim, Germany, mario.grau@hs-rm.de

Abstract: A high performance MEMS Pirani sensor, called VAC_03, was designed and optimized by analytics [1]. Due to the fact that this MEMS Pirani sensor is a 3D-Object, the calculation of the thermal radiation by simplified analytical models is very limited. As the radiation behavior in the system is, beside the solid thermal conductance, responsible for the detection limit of such thermal conductivity vacuum gauges, we switched to a FEM-Software for analyzing the actual 3D-geometry. This way all view factors of the interacting surfaces can be precisely calculated. Solid heat conduction is calculated straight forward by Fourier heat transfer. Gaseous heat flux calculation is based on analytical equations. The developed FEM-Model represents the measurement performance of the sensor precisely. Hence, we use the model for further geometric optimization by systematically sweeping crucial parameters. This way we can approximate the gain in sensitivity related to the technological effort.

Keywords: heat transfer, parametric sweep, equation based modeling, MEMS, Pirani sensor, thin-film resistor

1. Introduction

Pirani sensors are based on a heating and sensing element or a combined element as in this case. The electrical heating power is dissipated by solid head conduction, gaseous heat conduction and by thermal radiation. Only the gaseous heat losses are pressure-dependent. However, for some electrical configurations the working temperature of the heating element is a function of pressure *p*. Hence, the radiation losses vary with the pressure *p* as well as they strongly depend on the temperature difference between heated element and environment. The analytical model did not show a sufficient precision in modeling the radiation in the system, so we switched to COMSOL Multiphysics.

2. Sensor Design

We use a meander shaped Ni resistor ($R(T)$) patterned onto a membrane, which is suspended by four 300 nm thin beams (see Figure 1). Membrane and beams consist of a stress compensated low-pressure chemical vapor deposition (LPCVD) silicon nitride (Si_3N_4). The membrane is suspended from a Si chip-rim above an etch groove. Onto the chip rim we pattern an additional Ni resistor (R_K) that shows the same electrical resistance, line width and temperature coefficient of resistance (TCR). On top of the chip rim we placed a silicon microbridge (Si-mb). This Si-mb has two functions. First, it is working as a radiation shield; secondly it acts as a nearby heat sink to increase the gaseous thermal conductance (see Figure 2).

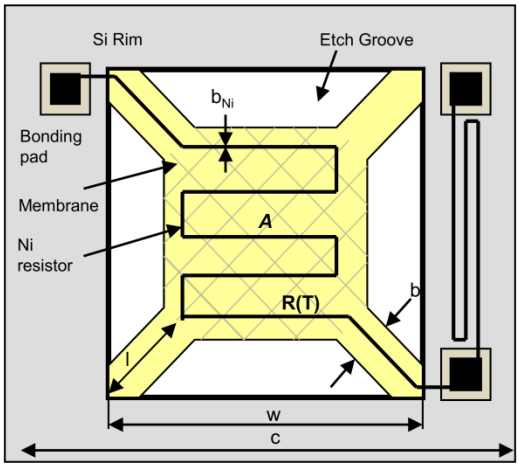

Figure 1. Schematic top view of the MEMS Pirani Sensor VAC_03.

The chip's main dimensions can be reviewed in Table 1.

3. Thermal Analysis

This chip design allows us to describe the sensor's performance by an analytical model, which is based on thermal conductances. In fact,

we used this model for designing and optimizing the sensor. This section summarizes the basic assumptions and equations used for modeling. We assume that the membrane area A is heated homogenously. A temperature gradient can be found on each of the four beams only. For calculating the gaseous heat conductance, we work with two cylindrical shaped gas volumes below and above the membrane with the same (base) area A and a height d_1 and d_2, being the distances to the heat sinks, respectively. With this simplification an error is induced, which we compensate by a correction factor that is multiplied with the gaseous thermal conductance. The radiative heat losses are approximated by the Stefan-Boltzmann law as well as the Kirchhoff's law of radiation. We only take the reflecting surfaces below and above (radiation shield and transistor-outline header) into account.

As the model is a thermal conductance based one, the following equation describes the main relations:

$$T - T_0 = N/(G_c + G_r + G_g)$$

in a simple but sufficient way. T, T_0 and N denote the membrane's temperature, the heat sink's as well as the ambient temperature and the electrical power used for heating the Ni resistor, respectively. The three conductances G_c, G_r and G_g represent the solid thermal conductance, the radiative thermal conductance and the gaseous thermal conductance. In Table 2 one can review the equations used to describe the thermal conductances in this model.

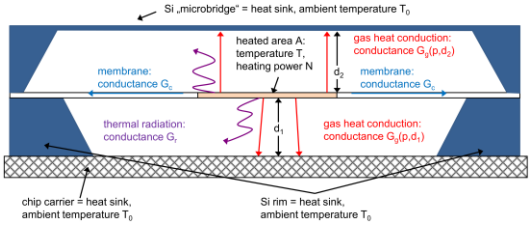

Figure 2. Schematic cross section of the MEMS Pirani Sensor.

The solid thermal conductance G_c consists of two terms, one respecting the four beams, the second one respecting the two parts of the Ni resistor, which enters and leaves the membrane via two of the four beams. The radiation losses and therefore G_r depends on the temperature difference between membrane and environment, the area of the membrane A and the emissivity of the membrane's surface ε (see Table 2). The gaseous conductance $G_g(p)$ depends on gas specific properties (e.g. the accommodation coefficient a and the mean free path $\bar{l}(p)$ of the gas molecules). According to Wutz[2] the thermal conductivity λ of gases can be approximated in all pressure regimes by the following equation:

$$\lambda(p,d) = \lambda(p_0)\left(1+2\left(\frac{2-a}{a}\right)\frac{\bar{l}(p)}{d}\frac{9.5}{6}\right)^{-1}$$

For powering the sensor, we use a Wheatstone bridge circuit (see Figure 3). The electrical power N can be described by the resistor's ratios and the bridge supply-voltage U_b (see Table 2). By using the expression for the thermal conductances and respecting the electrical power injected into the measuring resistor, one can approximate the temperature difference by iteration. This function $T(p)$ can be transformed to a signal voltage $U(p)$ by taking the electronic configuration into account.

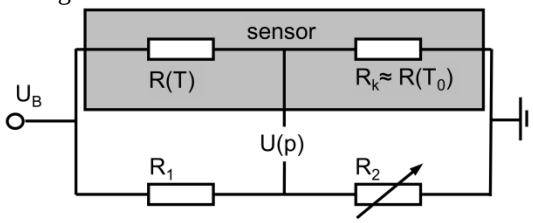

Figure 3. Schematic representation of the bridge circuit powering the MEMS Pirani Sensor.

A simplified expression for $U(p)$ is given by:

$$U(p) \approx \frac{1}{4}\,ß\Delta T\left[1-\frac{ß\Delta T}{2}+\left(\frac{ß\Delta T}{2}\right)^2\right]U_B,$$

with β denoting the TCR of the nickel thin-film resistor. This equation implies a signal increase for higher membrane temperatures. But the sensors sensitivity is defined by dU/dp. From this it follows that if the temperature is increased, the absolute signal voltage rises, but the sensitivity decreases in the high-vacuum range. The reason for this is the strong temperature dependency of the radiative thermal conductance G_r. G_r and G_c dominate in the lower pressure range; hence both conductances have to be minimized. As one can see in Table 2, there are

material properties and geometric parameters inside the expressions. Many of these can be modified technologically. By performing parameter sweeps with COMSOL Multiphysics, we can optimize the increase in sensitivity compared to the technological effort needed. A more detailed description of this analytical model can be found in [1].

4. Use of COMSOL Multiphysics

For creating the geometry of the sensor we used COMSOL's Standard CAD-Module. The chip's geometry is fully represented in 3D with exact physical dimensions. Most characteristic parameters can be changed without breaking the geometry or meshing sequence.

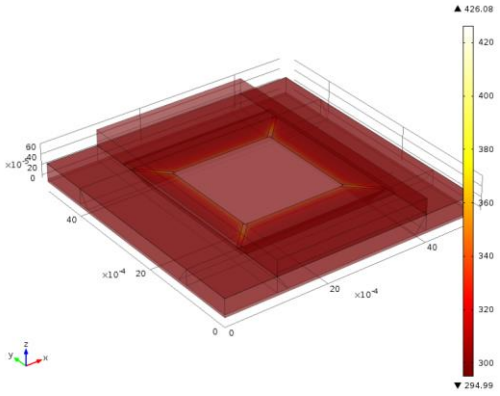

Figure 4. 3D model of the MEMS Pirani Sensor VAC_03, Si-mb on top of the chip rim is represented semi-transparent, heat-flux gradients can only be found along the beams and in the gas volumes.

All the main parts as the edge length of the membrane and beams, as well as the chip-rim dimensions can be swept. The remaining sizes are calculated out of these customized parameters. Even the distance between Si-mb and membrane as well as the thickness of beam and membrane are parameterized. This way we are able to study the impact of geometric design-optimization on the sensor's sensitivity.
In order to keep the calculation time reasonable, we use the following assumptions and simplifications:

- The meander is not geometrically represented. The membrane is defined as heat source.
- There is no convection in the system. The gas volumes are of stationary kind.
- Gas volumes are fully transparent to any kind of radiation.
- The surface emissivities show no temperature dependency.
- The 300 nm thin edges of membrane and beams are set up with adiabatic boundary-conditions.

The first simplification can be done without hesitation due to the fact that we deposit an Au layer onto both sides of the membrane. This way we reduce the membranes emissivities ε, hence the radiation losses are decreased. Additionally, the Au layer generates a homogenous heat distribution throughout the membrane area. The second and third simplification is logical when using a solid body as gas volume with pressure-dependent heat conductivity (we are using the equation of the analytic model, as it works for molecular, transitional and viscous pressure regimes). The last simplification has virtually no effect on the solution at all, as these surfaces are arbitrarily small compared to the remaining ones. All surfaces inside the cavity and between Si-mb and membrane are set up to surface-surface radiation. The outer surfaces radiate to the environment.

The membrane is configured as heat source and the equation for the power N (see. Table 2) is used as value for the "total power" of the heat source. This way we take the electrical circuitry into account.

In order to respect the Ni meander segment that is patterned onto two of the four beams we create a new thermal conductivity for those two beams. As the product of thickness d and thermal conductivity λ can be seen as constant (with thermal conductance in mind), we sum the $d\lambda$-products of the Ni and the Si_3N_4, and divide this by the silicon nitride's thickness. This way we get a new thermal conductivity, which respects the Ni conductor without actually having a geometric representation implemented into the model.

5. Results

In Figure 5 a chart shows a comparison between measured and simulated data. The *T(p)* function calculated by COMSOL is transformed by an analytic expression to the signal voltage

function *U(p)*. The sophisticated model shows a good agreement in the high vacuum as well as in the lower fine-vacuum range. The most sensitive area, found in the range between 10^{-4} and 10^{-2} Torr, slightly differs from the measurements. That is mainly caused by the unknown accommodation coefficient of the gas *a*. We used a value for nitrogen on smooth platinum surfaces (a=0.77, [2]), because there are no matching measurements for smooth Au surfaces found in literature.

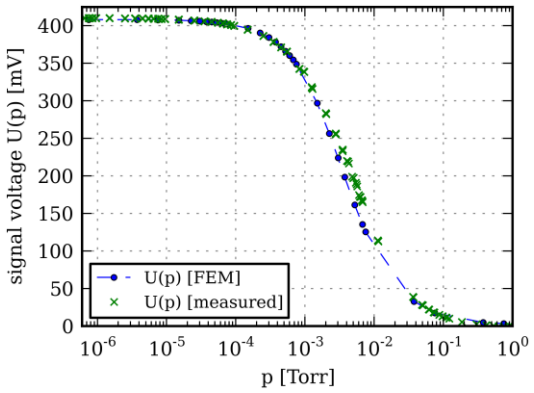

Figure 5. Signal voltage *U(p)* of simulated and measured data.

The purpose of the VAC_03 is to show an increased performance in the high vacuum. Hence, we have to increase the gaseous thermal conductance as far as possible. The obvious way for doing this is an enlargement of membrane area *A*. An inevitable side-effect is that at the same time the radiation losses and solid thermal conductance (for a given chip-rim size) are increased as well.

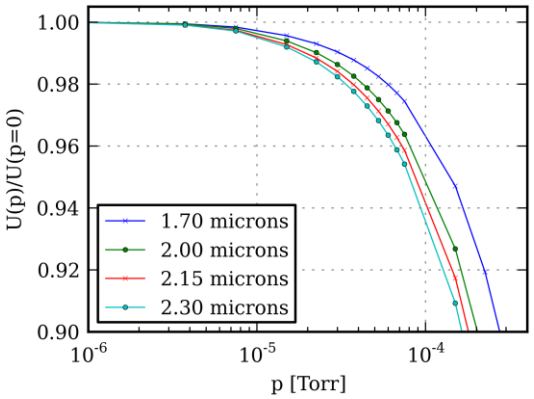

Figure 6. Signal voltage *U(p)* normalized to unity of simulated data for a parametric sweep of the membrane's edge length.

The decision for the 2000 µm edge length in combination with 746 µm long beams is based on analytics. An optimal ratio can be calculated (if all conductances are known precisely). The FEM results support that analytical optimum-value in showing a decreasing improvement for constantly enlarging the membrane area. Although these results also indicate that a slightly larger membrane could still increase the sensor's performance in the high-vacuum range (see Figure 6). However, by further increasing area *A*, we also reduce the sensitivity in the fine and rough vacuum. As the gas cooling is more efficient, the temperature increase we get for a given bridge supply-voltage is flattened. A membrane size of 4 mm^2 represents a good choice for a decent performance in the high and fine vacuum for a constant supply-voltage. In a similar way we studied the influence of several crucial parameters on the sensor performance (see Table 3) in specific pressure ranges.

6. Conclusions

FEM simulations are powerful tools for optimizing and developing complex prototypes of many kinds. In most cases, especially for 3D systems, analytical models have to be much simpler. As FEM-Software's precision often scales with computational power, it is far more suited for designing and developing non-idealized real-world prototypes. We designed a MEMS Pirani Sensor by analytics, called VAC_03. This sensor is optimized for the fine- and high-vacuum range. This optimization for the high vacuum is based on studying parasitic thermal conductances, meaning the solid and the radiative thermal conductances in this case. By using COMSOL Multiphysics, we are able to analyze the radiation behavior and the impact of design optimization much deeper as analytics would allow.

7. References

[1] F. Völklein, M. Grau et al., J. Vac. Sci. Technol. A 31, 061604 (2013)
[2] M. Wutz, H. Adam, and W. Walcher, Handbuch Vakuumtechnik (Vieweg, Wiesbaden, 1997)

8. Appendix

Table 1: Geometrical dimensions of VAC_03

A	4 mm^2
w	3000 µm
l	746 µm
b	70 µm
$\mathbf{b_{Ni}}$	12 µm
$\mathbf{d_{Ni}}$	200 nm
$\mathbf{d_M}$	300 nm

Table 2: Analytic equations

$G_g(p) = \lambda(p, d_1)\frac{A}{d_1} + \lambda(p, d_2)\frac{A}{d_2}$
$G_c = 4\frac{\lambda_{Si3N4} d_M b}{l} + 2\frac{\lambda_{Ni} d_{Ni} b_{Ni}}{l}$
$G_r = \frac{2\varepsilon\sigma(T^4 - T_0^4)A}{(T - T_0)} =$ $8\varepsilon\sigma T_0^3 A\left[1 + \frac{3}{2}\frac{\Delta T}{T_0} + \left(\frac{\Delta T}{T_0}\right)^2 + \frac{1}{4}\left(\frac{\Delta T}{T_0}\right)^3\right]$ $\approx G_{r0}\left[1 + \frac{3}{2}\frac{\Delta T}{T_0} + \left(\frac{\Delta T}{T_0}\right)^2\right]$
$N = \left(\frac{R(T)U_B}{R_K + R(T)}\right)^2 \Big/ R(T) = \frac{U_B^2}{4R_K}\frac{(1 + ß\Delta T)}{(1 + ß\Delta T/2)^2}$

Table 3: Parametric sweeps

• Distances d_1 and d_2 • Chip rim width   • Beam length/width   • Membrane size   • Material properties (TCR, λ)   • Bridge supply-voltage